Development changes in multi-scale structure and functional properties of waxy corn starch at different stages of kernel growth

Bo Zheng, Xinbo Guo, Yukuo Tang, Ling Chen, Fengwei Xie

PII: S0141-8130(21)02048-1

DOI: https://doi.org/10.1016/j.ijbiomac.2021.09.120

Reference: BIOMAC 19419

To appear in: *International Journal of Biological Macromolecules*

Received date: 11 July 2021

Revised date: 2 September 2021

Accepted date: 18 September 2021

Please cite this article as: B. Zheng, X. Guo, Y. Tang, et al., Development changes in multi-scale structure and functional properties of waxy corn starch at different stages of kernel growth, *International Journal of Biological Macromolecules* (2018), https://doi.org/10.1016/j.ijbiomac.2021.09.120

Development changes in multi-scale structure and functional properties of waxy corn starch at different stages of kernel growth

Bo Zheng[1], Xinbo Guo[1], Yukuo Tang[1], Ling Chen[1,*], Fengwei Xie[2,**]

[1] Ministry of Education Engineering Research Center of Starch & Protein Processing, Guangdong Province Key Laboratory for Green Processing of Natural Products and Product Safety, School of Food Science and Engineering, South China University of Technology, Guangzhou 510640, China

[2] International Institute for Nanocomposites Manufacturing (IINM), WMG, University of Warwick, Coventry CV4 7AL, United Kingdom

*Corresponding author. felchen@scut.edu.cn; Tel: +86 20 8711 3252 (L. Chen)

**Corresponding author. d.xie.2@warwick.ac.uk; fwhsieh@gmail.com (F. Xie)

Abstract

Waxy corn starch is widely used in food and papermaking industries due to its unique properties. In this work, the structural and functional properties of starch isolated from waxy corn at different stages of kernel growth were investigated and their relationships were clarified. The results showed that with kernel growth, the surface of starch granules became smooth gradually, and the inner growth rings and the porous structure grew and became clear. Meanwhile, the weight-average molecular mass (M_w), root mean square radius (R_g), and average particle size increased while the amylose content decreased, which should account for the decreased pasting temperature (from 71.37 to 67.44 °C) and increased peak viscosity (1574.2 to 1625.1 cp) and breakdown value observed. Besides, the contents of slowly digestible starch (SDS) and resistant starch (RS) in waxy corn starch decreased significantly (from 44.01% to 40.83% and from 16.73% to 9.80%, respectively, $p < 0.05$) due to decreases in the double helix content, crystallinity, structural order, and increases in the semi-crystalline lamellae thickness and the amorphous content. This research provides basic data for the rational utilization of waxy corn starch at different stages of kernel growth.

Keywords

Waxy corn starch; kernel growth; starch structure; pasting properties; starch digestibility

1. Introduction

Waxy corn is a corn cultivar whose nutritional composition is similar to that of regular corn, with a starch content of 64–68%, a protein content of 10–15%, a fat content of 4–5%, and a vitamin content of about 3% [1]. Starch, mainly amylopectin, is the main component of waxy corn, and waxy corn starch (WCS) has different physical and chemical properties from those regular corn starch (containing a certain amount of amylose), such as improved paste stability, higher paste transparency and reduced tendency of retrogradation [2, 3]. Due to these natural properties, WCS has been widely used as different types of food additives such as thickeners and stabilizers [4-6]. However, WCS also has high rapidly digestible starch (RDS) content and thus it could be easily digested into glucose leading to elevated blood glucose [7]. Therefore, one of the research focuses nowadays is to use "green" methods to modify the physical and chemical properties of WCS to meet wider application needs [8, 9]. Among them, genetic modification by biological means to change the formative and metabolic pathways of WCS from the original source and then to regulate its functional properties has become the frontier research direction in agriculture, food and materials areas [10].

The functional properties of starch are determined by its multi-scale structure [11]. Therefore, in order to regulate the functional properties of WCS from the perspective of gene modification, it is necessary to master the variation of its multi-scale structure and properties during different stages of kernel growth and to understand the structure–property relationships. Previous studies have shown that during the growth of grain kernels, the synergistic effects of various starch biosynthetases would result in evolution in the molecular structure, molecular weight and distribution, and the short-range ordered structure and helical arrangement of starch molecules in starch grains, which might lead to

change in starch aggregated structures (e.g. particle structure, lamellar structure and crystalline structure) [12-14]. The changes in lamellar structure, crystallinity, and granule size, mainly associated with starch branched chains, at different stages of kernel growth eventually affect the functional properties such as the thermal properties, pasting properties, and digestibility of starch [15]. A structural study suggested that the granule size of WCS increased with kernel growth, which led to increasing pasting peak viscosity [16]. Similarly, another study showed that the average chain length distribution of WCS amylopectin increased with kernel growth, and the WCS at harvesting exhibited the lowest peak viscosity, which then increased post-harvesting [16]. Therefore, WCS at different stages of kernel growth has different structural and functional properties.

Though there have been many systematic studies on the multi-scale structure and functional properties of WCS [17-19], there have been limited comprehensive studies on the changes of multi-scale structure and functional properties of WCS during kernel growth, especially their relationships. Besides, for the waxy corn, the flowering and grain period is generally 20–30 days after pollination, which is the best harvest period. In this period, the reproductive growth of waxy corn grains begins instead of vegetative growth, and the structure of starch might change significantly. Thus, in this work, the multi-scale structure (granule structure, short-range molecular order, helices, molecular mass and distribution, lamellar structure, and crystalline structure), pasting properties, and *in vitro* digestibility of starch isolated from waxy corn at different stages of kernel growth (20, 25, 30, and 35 days after pollination) were investigated. In this way, the relationship between the structure and functional properties of WCS during kernel growth can be clarified. These results could provide basic data for the rational utilization of WCS at different stages of kernel

growth.

2. Materials and methods

2.1 Plant materials

Waxy corn was planted at the Zhong Luotan Experimental Base of the Guangdong Academy of Agricultural Sciences (Guangzhou, China). The kernels collected on the 20th, 25th, 30th and 35th day after pollination during the growth stages of waxy corn were selected as experimental samples (named as 20DAP, 25DAP, 30DAP and 35DAP, respectively) for starch extraction.

2.2 Isolation of WCS

The well-developed kernels of 20DAP, 25DAP, 30DAP and 35DAP were selected, and the starch was extracted from waxy corn according to a previous study [20]. Firstly, the kernels were mixed with 0.45% sodium metabisulfite in a ratio of 1:2 (w/w) and soaked for 12 h, and treated with a beater for 30 s. After filtration through a layer of gauze, the filtrate was passed through screens of 80 mesh, 100 mesh, and 200 mesh, respectively. The filtrate was then collected and centrifuged at 4000 rpm for 10 min. After that, the supernatant was discarded, and the precipitate was centrifuged with sufficient water and absolute ethanol three times and once respectively. The following steps included decolorization to no pigmentation, filtration, drying (35 °C, overnight), and grinding (80 mesh) to obtain 4 samples (20DAP, 25DAP, 30DAP and 35DAP) for use. After isolation, the chemical compositions of four starch samples were shown in **Table 1**.

2.3 Scanning electron microscopy (SEM)

The starch samples were evenly dispersed on the sample table with the conductive double-sided tape, and then the unstuck starch was blown away. The samples were sputter-coated with gold for 5

min. The SEM examined was used by an EM-30 Plus scanning electron microscope (COXEM, Korea) operated at 20 kV with 500× magnification.

2.4 Confocal laser scanning microscopy (CLSM)

Starch was stained using a method used in our previous study [21], in which a freshly prepared APTS (8-amino-1,3,6-pyrenetrisulfonic acid) acetic acid solution (10 mM) was used as the dye. After staining, a drop of the starch suspension was transferred to a glass slide, covered with a coverslip, and then observed with a Digital Eclipse Cl Plus confocal microscope (Leica, Germany). The lenses were HC PL APO CS2 63 × 1.40 OIL, and the laser emission wavelength of the Ar/Kr gas laser was 488 nm (20% capacity), accompanied by a receiving wavelength range of 480–500 nm. For each starch sample, images (resolution 1024 × 1024 pixels) of a stack of horizontal optical sections (thickness 0.5 μm) were obtained, encompassing the whole starch granule in three dimensions. Then, these images were superimposed together using Image J to construct the structure diagram of growth rings in starch granules.

2.5 Granule size analysis

The starch samples were loaded into the reservoir until completely dispersed in anhydrous ethanol. The granule size distribution of starches was determined using a laser-diffraction analyzer (Malvern Mastersizer 2000, UK) with a flow-through reservoir (1000 mL). The obscuration value was 12–13% and the refractive index of starch samples was 1.52. All the measurements were analyzed in triplicate.

2.6 Amylose content (AC)

Amylose content (AC) was determined based on iodine-binding capacity as described

previously [22]. Specifically, starch (100 mg, dry basis) was dispersed in 1 mol/L NaOH and diluted with distilled water to obtain a 1 mg/mL solution. I_2/KI solutions (0.0025 mol/L I_2 and 0.0065 mol/L KI) were used to complex with starch, and the absorbance of all samples was measured using a UV–vis spectrophotometer (Evolution 201 UV–Visible Spectrophotometer, Thermo Scientific Inc., Waltham, USA) at 620 nm. AC was determined using a standard curve based on the mixtures of the standard amylose solutions and the standard amylopectin solutions of different concentrations.

2.7 Gel permeation chromatography coupled with multi angle light scattering (GPC-MALS)

Weight-average molecular molar mass (M_w), number-average molecular mass (M_n), and gyration radius (R_g) were determined as did in our previous study [23]. The starch sample was dissolved in DMSO containing 50 mol·L^{-1} LiBr to achieve a mass concentration of 0.5 mg·mL^{-1}. Then, the fully dissolved starch sample was filtered through a 5-μm PTFE filter film (Millipore Co., Billerica, USA) and transferred to a vial for testing. A GPC system (Waters, USA) equipped with a MALLS detector (Wyatt Technology Co., Santa Barbara, USA) and a refractive index detector was used. Two GPC columns (SB-804 and SB-806) with a flow rate of 1 mL·min^{-1}, a detection wavelength of 658.0 nm, and an injection volume of 100 μL at 25 °C were used.

2.8 Fourier transform infrared (FTIR) spectroscopy

FTIR analysis was carried out on a Nicolet iS50 infrared spectrometer (Thermo Fisher, Waltham, USA) equipped with an ATR single-reflectance cell following our previous study [23].

2.9 Solid-state cross-polarization magic angle spinning carbon-13 nuclear magnetic resonance (CP/MAS ^{13}C-NMR) analysis

Solid-state CP/MAS ^{13}C-NMR analysis was performed on a Bruker AVANCE III HD 400 spectrometer (Bruker, Germany) equipped with a 4-mm broadband double-resonance MAS probe following our previous procedure and conditions (100.613 MHz and 295 K) [23]. Over 6000 scans were recorded for a spectrum and the recycle delay was 2 s. The spectra were analyzed using PeakFit v4.12 software.

2.10 X-ray diffraction (XRD)

XRD analysis was measured by a powder X-ray diffractometer (PANalytical Co., Almelo, Netherlands) with Cu-Kα radiation at 40 mA and 40 k following our previously established conditions (scanning over a 2θ range of 5–35° at a speed of 10°/min and a step size of 0.033°) [24]. MDI Jade software (Version 6.0) was used to calculate relative crystallinity (RC) following our previous study [24].

2.11 Small-angle X-ray scattering (SAXS)

SAXS analysis was performed on a SAXS system (Anton Paar, Graz, Austria) following our previously established conditions (Cu-Kα radiation source, 50 mA, 40 kV, and 0.1542 nm wavelength) [25]. All data generated were normalized and further processed using SAXS quant 3.0 software.

2.12 Pasting properties

The pasting properties of different starch samples were determined following our previous study [22]. A starch suspension (20 g, concentration 6%, w/w, dry basis) was prepared and transferred into

the testing unit of an MCR302 rheometer (Anton Paar, Austria). Starch samples were heated from 30 to 95 °C at 7.5 °C/min, held at 95 °C for 30 min, cooled from 95 °C to 50 °C at 7.5 °C/min, and then held at 50 °C for another 30 min. The viscosity curves of starch with time and temperature were obtained.

2.13*In vitro* starch digestibility

The *in vitro* digestibility of WCS was assessed by the Englyst method with slight modification as reported previously [25]. Briefly, porcine pancreatin (12 g, 1.4×10^4 USP) was suspended in 80 mL water and stirred for 30 min. After centrifugation at 4000 g for 20 min, 54 mL of the supernatant was collected. Amyloglucosidase (3.15 mL, 45 units) was dissolved into 3.85 mL of deionized water and 6 mL of solution collected was mixed with the 54 mL of the supernatant. The solution should be freshly prepared before use.

1 g of starch was mixed with 20 mL of 0.1 M acetate buffer (pH 5.2) in a flask, cooked in a boiling water bath for 30 min with continuous stirring and then cooled at 37 °C. Subsequently, an enzyme solution (5 mL) was added and incubated at 37 °C in a water bath. After 20 and 120 min, the hydrolysate (0.5 mL) was removed and mixed with 20 mL of 70% ethanol. The samples were centrifuged at 4000 g for 6 min and the hydrolyzed glucose concentration of the supernatant was measured using a GOPOD reagent. The glucose content after 20 and 120 min of hydrolyzation was labeled as G20 and G120, respectively. The glucose concentration at 20 min and 120 min was used to calculate the contents of rapidly digestively starch (RDS), slowly digestive starch (SDS), and resistant starch (RS) using the equations below:

$$RDS = (G20 - FG) \times 0.9$$

$$SDS = (G120 – G20) \times 0.9$$

$$RS = TS – (RDS + SDS)$$

where G20 and G120 represent glucose concentrations at 20 min and 120 min respectively, FG the initial glucose concentration, and TS the content of starch. Each sample was analyzed in triplicate.

2.14 Statistical analysis

All tests were conducted at least in triplicate, and data were analyzed using IBM SPSS statistics version 22.0 (IBM, Armonk, NY, USA). Analysis of variance (ANOVA) was performed for each characteristic followed by Duncan's multiple-range test; data were expressed as mean values ± standard deviation (SD), and the least significant difference was set to compare mean differences at $p < 0.05$.

3 Results

3.1 Granule morphology and granule size distribution

Fig. 1 shows the SEM images of WCS at different growth stages, and their granule sizes are presented in **Table 2**. The WCS granules at different growth stages were polygonal or round in uneven size with multiple planes or edges. With the growth of kernels, the granules became full, and their surface was smoother. Meanwhile, depressions were gradually repaired and disappeared to form mellow and complete granules. Furthermore, the average starch granule size increased gradually and reached 12.203 μm for 30DAP. For 20DAP, the starch granules had not grown completely, which appeared to be hollow and sag, along with a smaller granule size. The average starch granule size reached 12.1 μm for 35DAP, which is consistent with a previous study [26].

3.2 Granule internal structure

CLSM is one of the most effective methods to investigate the internal structure of starch granules [27]. Growth rings, formed by the accumulation of crystalline and amorphous lamellae during growth, can be shown by alternating light and dark layers under CLSM (**Fig. 2**). Up to 20 days of growth, growth rings were not obvious. With a longer period of growth, growth rings gradually became clear, and for 35DAP, growth rings became integral and distinct. Besides, for 20DAP, the internal porous channels of starch granules were short and fuzzy. With the growth of kernels, radiation fringes gradually developed in the outer layer and the number of radiation fringes increased, indicating there were more channels and these channels became longer. For 35DAP, more channels extending from the umbilical point to the edge were formed. Previous studies showed that more channels are observed in waxy corn starch than in high-amylose corn starches (Gelose 50 and Gelose 80), and these channels are more distinct. Meanwhile, the channels were visible as dark lines running from the border of the granule toward the hilum in WCS, which were consistent with our results [28].

3.3 Molecular molar mass

The molecular mass and molecular mass distribution of WCS at different time points during growth were determined and the results are shown in **Table 2**. Interestingly, with the prolongation of kernel growth, and both M_w and M_n decreased firstly and then increased, meanwhile the molecular mass distribution first narrowed and then widened. In this regard, we proposed that during growth, the molecular chains of WCS decomposed first, followed by polymerization. This phenomenon is worth further investigation. For 35DAP, it reached 5.225×10^7 g/mol and 4.895×10^7 g/mol,

respectively ($p < 0.05$). For 20DAP, the proportion of chains with M_w below 5×10^7 g/mol was 94.23%, which was the highest among these four samples. However, for 35DAP, most of the starch molecules were in the region of 4–5×10^7 g/mol. Furthermore, with the kernel growth until day 30, there were no chains with M_w beyond 6×10^7 g/mol. But further growth until day 35 led to the molecular mass distribution dominating at higher values and higher M_w and R_g values for 35DAP. Besides, with the growth of kernels, the AC had a downward trend and the lowest AC was 1.20% for 35DAP ($p < 0.05$).

3.4 Short-range ordered structures

FTIR is very sensitive to the conformation of chains and helical structures, which can quantitatively reflect the proportion of ordered and amorphous structures in starch [22]. For the different starch samples, the FTIR spectra before and after deconvolution are shown in **Fig. 3A** and the ratios of peak intensities at 1045 cm^{-1} and 1022 cm^{-1} ($R_{1045/1022}$) were listed in **Table 3**. During kernel growth, the $R_{1045/1022}$ value for WCS decreased continuously, which shows that the short-range order of WCS decreased continuously and reached the lowest for 35DAP ($p < 0.05$).

The CP/MAS ^{13}C NMR spectra of starch samples were used to further analyze the short-range structures (single- and double-helices). It can be seen from **Table 3** that the double helix content of WCS showed a downward trend ($p < 0.05$) with kernel growth. For 20DAP, the mass fraction of amorphous starch was 47.7%, that of V-type single helices was 5.9%, and that of double helices was 46.4%. In the sample of 35DAP, amorphous starch accounted for 59.4% and double helices 40.6%, while there were no V-type single helices. This indicated that the single helix structure had appeared in the starch granules before the 20th day. The 35DAP sample had the minimum content of double

helices (40.6%) and the highest amorphous content (59.4%).

3.5 Crystalline structure

Fig. 3B shows the XRD patterns of four WCS samples. The peaks centered in the 2θ region of 10°–30° indicated the crystallizability of WCS, similar to the reported XRD patterns of starches from waxy corn [7]. Moreover, **Fig. 3B** shows that all the starch samples displayed strong diffraction peaks at 15.1°, 17.1°, 18.0° and 23.0°, indicating the A-type crystalline structure [29]. **Table 3** shows that during the growth of WCS, the RC of starch decreased significantly with kernel growth (p < 0.05) while the crystalline structure did not change significantly. In particular, when the corn starch grew from day 30 to day 35, the RC decreased from 32.5% to 30.7%. This may be due to the action of related enzymes during growth, resulting in the unwinding of helices and the disruption of starch chain arrangement. It could also be possible that starch in an amorphous state was mainly formed during the later stage of kernel growth.

3.6 Lamellar structures

The lamellar structure of WCS at different kernel growth stages was analyzed by SAXS (**Fig. 3C**) and the related parameters are listed in **Table 3**. All the starch samples had a distinct scattering peak at around q = 0.652–0.670 nm^{-1}. According to the Woolf-Bragg equation $d_{Bragg} = 2\pi/q$, the average repeat distance (d_{Bragg}) in WCS at different growth stages was calculated to be between 9.33 and 9.64 nm, with a slightly upward trend. The thicknesses of starch crystalline lamellae (d_c), amorphous lamellae (d_a), and semicrystalline lamellae (L) were also obtained from SAXS curves by the one-dimensional correlation function (**Fig. 3D**). The results (**Table 3**) show that with kernel growth, L and d_c increased especially for 35DAP (p < 0.05), while d_a first decreased and then

increased. Clearly, the growth of starch molecular chains resulted in the arrangement of helices to form crystalline lamellae especially in the later stage of kernel growth.

3.7 Pasting properties

The pasting properties of starch are commonly caused by changes in viscosity during the heating and cooling cycle of starch dispersions in water, which were significantly correlated with amylose leaching, crystallinity and chain length of starch [30, 31]. The starch gelatinization characteristics of WCS at different growth stages are shown in **Fig. 4** and **Table 4**. The pasting temperature (T_p) of 20DAP was 71.37 °C. With the kernel development, the starch samples showed a lower pasting temperature, due to the enhanced long- and short-range ordered structures. Accounting for this, the disaggregation of starch orders (crystal structure and short-range ordered structure) could decrease the thermal stability which was consistent with our previous study [32]. The peak viscosity (η_{pk}) showed an upward trend, and it reached the maximum for 35DAP. This phenomenon can be explained by the formation of long side chains with similar molecular mass (**Table 2**). After gelatinization, long starch chains were prone to undergo chain entanglement, leading to increased peak viscosity [33, 34]. Besides, the thermostability of starch paste decreased, while its cold stability increased, which may also be linked to the growing chain structure. Moreover, the kernel development resulted in a noticeable increase in the setback value (η_{sb}, from about 147 to 211 cP), which may be due to the reduction trend of short chains following the lack of aggregation and entanglement [35].

3.8 *In vitro* digestibility

The nutritional function of starch depends on its digestibility, which is the primary factor

affecting the postprandial glucose and insulin responses [36, 37]. The *in vitro* digestibility of starch from different growth stages was analyzed with the results shown in **Table 3**. The contents of RDS, SDS and RS for 20DAP were 40.26%, 44.01%, and 16.73%, respectively. With the prolongation of kernel growth, the RDS content of WCS increased significantly, while the SDS and RS contents decreased significantly, and the trend of the RS content was in line with plantain (Musa ABB) starch [30]. For 35DAP, the RDS content increased to 49.30%, the SDS content decreased to 40.88%, and the RS content decreased to 9.80%. Research [38] suggested that the amorphous parts in WCS granules could be easily hydrolyzed by amylase and were the main components of RDS. Moreover, a small number of single helices and double helices with high perfection, the highly ordered crystalline structure, and the crystalline regions in the semi-crystalline lamellar structure, all constitute the RS portion of WCS, while some parts of imperfect crystalline structure compose the SDS portion, as confirmed by the helices, short-range order, RC, and lamellar structure results in **Table 3**. In this current study, we found that during kernel growth, the amorphous structure, ordered structure and crystalline structure of starch changed significantly, and the content of double helices showed a downward trend. The single helix content decreased to 0% for 25DAP. In general, kernel growth leads to a higher proportion of imperfect aggregated structures or amorphous structure which were more readily hydrolyzed by amylase, which accounted for the higher content of RDS and lower contents of SDS and RS (**Table 3**).

3.9 Correlations

The Pearson correlation coefficients of starch structure and digestive properties are presented in **Fig. 5A** in the form of a heatmap. The AC was significantly positively correlated with the RS and

SDS contents, and was significantly negatively correlated with the RDS content, suggesting the contribution of amylose to the digestion resistance of starch. The features of ordered structures such as RC and the content of V-type single helices had a significant positive correlation with the RS content and a significant negative correlation with the RDS content, while no significant correlation with SDS was shown. Besides, the double-helix structure was significantly positively correlated with the RS content. These correlations suggest that highly ordered starch structures (crystals and helices) are not readily digestible and is the main contributor to the digestion resistance of starch. A previous study showed that the RC of starch increased after diluted acid treatment, which decreased the starch digestibility [39]. Also, our previous work showed that the SDS and RS contents of modified starch samples were positively correlated with the double helix content and RC [25], which partly agrees with our results here. Moreover, R_g and amorphous starch content were significantly positively correlated with the RDS content, but were significantly negatively correlated with the RS and SDS contents, implying the disorderly arranged starch chains are susceptible to enzyme hydrolysis (**Fig. 5B**). Xu et al. reported that there was a positive correlation between RS and the double helix content and $R_{1045/1022}$, suggesting that the ordered structure formed by double helices and the compact short-range ordered structure had a major contribution to the digestion resistance of starch [7]. Overall, with kernel growth, the decreased ordered structure of WCS led to higher digestibility.

4 Conclusion

In conclusion, with the kernel growth, the semi-crystalline lamellae, crystalline structure, short-range ordered structures, and double-helical conformation of WCS all evolved, together with the variation in the starch chain structure. More specifically, the starch granules became full and

rounded, the length of molecule chains increased, the proportions of ordered structures ($R_{1045/1022}$, double helix, and RC) decreased, and the amorphous content increased. The changes in the starch ordered structures eventually led to the reduced retrogradation and improved starch digestibility. Therefore, the relationship between multi-scale structure, pasting properties and digestibility of starch isolated from waxy corn at different stages of kernel growth was established. The results provide basic data for controlling the multi-scale structure of starch at different growth stages, and then imparting better nutritional functions to starch.

5 Potential conflict of interest statement

The authors declare no competing financial interest.

6 Acknowledgements

This research has been financially supported by the National Natural Science Foundation of China under a General Project (No. 31871751 and 32101982) and the Key Project of the Guangzhou Science and Technology Program (No. 201804020036).

References

[1] A. Klimek-Kopyra, A. Szmigiel, T. Zajac, A. Kidacka, Some aspects of cultivation and utilization of waxy maize (Zea mays L. ssp. ceratina), Acta Agrobot. 65(3) (2012) 3-12.

[2] J.N. BeMiller, Chapter 19 - Corn Starch Modification, in: S.O. Serna-Saldivar (Ed.), Corn (Third Edition), AACC International Press, Oxford, 2019, pp. 537-549.

[3] I. Reddy, P.A. Seib, Modified Waxy Wheat Starch Compared to Modified Waxy Corn Starch, J. Cereal Sci. 31(1) (2000) 25-39.

[4] K. Rengsutthi, S. Charoenrein, Physico-chemical properties of jackfruit seed starch (Artocarpus heterophyllus) and its application as a thickener and stabilizer in chilli sauce, LWT--Food Sci. Technol. 44(5) (2011) 1309-1313.

[5] C.O. Moore, J.V. Tuschhoff, C.W. Hastings, R.V. Schanefelt, CHAPTER XIX - APPLICATIONS OF STARCHES IN FOODS, in: R.L. Whistler, J.N. Bemiller, E.F. Paschall (Eds.), Starch: Chemistry and Technology (Second Edition), Academic Press, San Diego, 1984, pp. 575-591.

[6] H. Zhang, L. Deng, Emulsifying Properties, in: Y. Fang, H. Zhang, K. Nishinari (Eds.), Food Hydrocolloids: Functionalities and Applications, Springer Singapore, Singapore, 2021, pp. 171-206.

[7] J. Xu, L. Chen, X. Guo, Y. Liang, F. Xie, Understanding the multi-scale structure and digestibility of different waxy maize starches, Int. J. Biol. Macromol. 144 (2020) 252-258.

[8] P. Mhaske, Z. Wang, A. Farahnaky, S. Kasapis, M. Majzoobi, Green and clean modification of cassava starch – effects on composition, structure, properties and digestibility, Crit. Rev. Food Sci. Nutr. (2021) 1-27.

[9] C. Guida, A.C. Aguiar, R.L. Cunha, Green techniques for starch modification to stabilize

Pickering emulsions: a current review and future perspectives, Curr. Opin. Food Sci. 38 (2021) 52-61.

[10] H. Gao, M.J. Gadlage, H.R. Lafitte, B. Lenderts, M. Yang, M. Schroder, J. Farrell, K. Snopek, D. Peterson, L. Feigenbutz, S. Jones, G. St Clair, M. Rahe, N. Sanyour-Doyel, C. Peng, L. Wang, J.K. Young, M. Beatty, B. Dahlke, J. Hazebroek, T.W. Greene, A.M. Cigan, N.D. Chilcoat, R.B. Meeley, Superior field performance of waxy corn engineered using CRISPR–Cas9, Nat. Biotechnol. 38(5) (2020) 579-581.

[11] C. Chi, X. Li, S. Huang, L. Chen, Y. Zhang, L. Li, S. Miao, Basic principles in starch multi-scale structuration to mitigate digestibility: A review, Trends Food Sci. Technol. 109 (2021) 154-168.

[12] Y. Zhong, J. Qu, A. Blennow, X. Liu, D. Guo, Expression Pattern of Starch Biosynthesis Genes in Relation to the Starch Molecular Structure in High-Amylose Maize, J. Agric. Food Chem. 69(9) (2021) 2805-2815.

[13] C. Martin, A.M. Smith, Starch biosynthesis, Plant Cell 7(7) (1995) 971-985.

[14] E. Li, J. Hasjim, E.K. Gilding, I.D. Godwin, C. Li, R.G. Gilbert, The Role of Pullulanase in Starch Biosynthesis, Structure, and Thermal Properties by Studying Sorghum with Increased Pullulanase Activity, Starch - Stärke 71(9-10) (2019) 1900072.

[15] S. Pérez, E. Bertoft, The molecular structures of starch components and their contribution to the architecture of starch granules: A comprehensive review, Starch - Stärke 62(8) (2010) 389-420.

[16] D. Ketthaisong, B. Suriharn, R. Tangwongchai, K. Lertrat, Changes in physicochemical properties of waxy corn starches at different stages of harvesting, Carbohydr. Polym. 98(1) (2013) 241-248.

[17] C.-S. Park, I. Park, The structural characteristics of amylosucrase-treated waxy corn starch and relationship between its in vitro digestibility, Food Sci. Biotechnol. 26(2) (2017) 381-387.

[18] C.M. Franco, C.F. Ciacco, D.Q. Tavares, The structure of waxy corn starch: effect of granule size, Starch- Stärke 50(5) (1998) 193-198.

[19] T.S. Rocha, S.G. Felizardo, J.-l. Jane, C.M.L. Franco, Effect of annealing on the semicrystalline structure of normal and waxy corn starches, Food Hydrocoll. 29(1) (2012) 93-99.

[20] X. Tan, B. Gu, X. Li, C. Xie, L. Chen, B. Zhang, Effect of growth period on the multi-scale structure and physicochemical properties of cassava starch, Int. J. Biol. Macromol. 101 (2017) 9-15.

[21] P. Bie, H. Pu, B. Zhang, J. Su, L. Chen, X. Li, Structural characteristics and rheological properties of plasma-treated starch, Innov. Food Sci. Emerg. Techno. 34 (2016) 196-204.

[22] K. Liu, B. Zhang, L. Chen, X. Li, B. Zheng, Hierarchical structure and physicochemical properties of highland barley starch following heat moisture treatment, Food Chem. 271 (2019) 102-108.

[23] Y. Liu, L. Chen, H. Xu, Y. Liang, B. Zheng, Understanding the digestibility of rice starch-gallic acid complexes formed by high pressure homogenization, I Int. J. Biol. Macromol. 134 (2019) 856-863.

[24] B. Zheng, T. Wang, H. Wang, L. Chen, Z. Zhou, Studies on nutritional intervention of rice starch- oleic acid complex (resistant starch type V) in rats fed by high-fat diet, Carbohydr. Polym. 246 (2020) 116637.

[25] T. Guo, H. Hou, Y. Liu, L. Chen, B. Zheng, In vitro digestibility and structural control of rice starch-unsaturated fatty acid complexes by high-pressure homogenization, Carbohydr. Polym. 256

(2021) 117607.

[26] N. Lindeboom, P.R. Chang, R.T. Tyler, Analytical, Biochemical and Physicochemical Aspects of Starch Granule Size, with Emphasis on Small Granule Starches: A Review, Starch - Stärke 56(3-4) (2004) 89-99.

[27] M.A. Glaring, C.B. Koch, A. Blennow, Genotype-Specific Spatial Distribution of Starch Molecules in the Starch Granule: A Combined CLSM and SEM Approach, Biomacromolecules 7(8) (2006) 2310-2320.

[28] P. Chen, L. Yu, G.P. Simon, X. Liu, K. Dean, L. Chen, Internal structures and phase-transitions of starch granules during gelatinization, Carbohydr. Polym. 83(4) (2011) 1975-1983.

[29] C. Les, B. Jaroslav, S. Hayfa, M.C. Tang, Form and functionality of starch, Food Hydrocoll. 23(6) (2009) 1527-1534.

[30] Y. Bi, Y. Zhang, Z. Gu, L. Cheng, Z. Li, C. Li, Y. Hong, Effect of ripening on in vitro digestibility and structural characteristics of plantain (Musa ABB) starch, Food Hydrocoll. 93 (2019) 235-241.

[31] B. Zhang, L. Chen, X. Li, L. Li, H. Zhang, Understanding the multi-scale structure and functional properties of starch modulated by glow-plasma: A structure-functionality relationship, Food Hydrocoll. 50 (2015) 228-236.

[32] H. Wang, Y. Liu, L. Chen, X. Li, J. Wang, F. Xie, Insights into the multi-scale structure and digestibility of heat-moisture treated rice starch, Food Chem. 242 (2018) 323-329.

[33] M. AlMaadeed, M. Ouederni, P.N. Khanam, Effect of chain structure on the properties of Glass fibre/polyethylene composites, Mater. Design. 47 (2013) 725-730.

[34] M.H. Madsen, D.H. Christensen, Changes in viscosity properties of potato starch during growth, Starch- Stärke 48(7- 8) (1996) 245-249.

[35] X. Chen, M. Chen, G. Lin, Y. Yang, X. Yu, Y. Wu, F. Xiong, Structural development and physicochemical properties of starch in caryopsis of super rice with different types of panicle, BMC Plant Biol. 19(1) (2019) 1-15.

[36] B. Zheng, T. Wang, H. Wang, L. Chen, Z. Zhou, Studies on nutritional intervention of rice starch-oleic acid complex (resistant starch type V) in rats fed by high-fat diet, Carbohydr. Polym. 246 (2020) 116637.

[37] J. Singh, A. Dartois, L. Kaur, Starch digestibility in food matrix: a review, Trends Food Sci. Technol. 21(4) (2010) 168-180.

[38] D. Qiao, F. Xie, B. Zhang, Z. Wei, S. Zhao, N. Meng, L. Rui, C. Qian, F. Jiang, Z. Jie, A further understanding of the multi-scale supramolecular structure and digestion rate of waxy starch, Food Hydrocoll. 65 (2017) 24-34.

[39] R.G. Utrilla-Coello, C. Hernández-Jaimes, H. Carrillo-Navas, F. González, E. Rodríguez, L.A. Bello-Pérez, E.J. Vernon-Carter, J. Alvarez-Ramirez, Acid hydrolysis of native corn starch: Morphology, crystallinity, rheological and thermal properties, Carbohydr. Polym. 103 (2014) 596-602.

Figure captions

Figure 1. SEM of waxy corn starch at different stages of kernel growth. (A) 20 DAP, (B) 25 DAP, (C) 30 DAP and (D) 35DAP: the kernels of the 20th, 25th, 30th and 35th day after pollination of waxy corn.

Figure 2. CLSM images of waxy corn starch granule (A) growth ring and (B) radial stripes (a–d, 20DAP, 25DAP, 30DAP and 35DAP: the kernels of the 20th, 25th, 30th and 35th day after pollination of waxy corn; e–h, 20DAP, 25DAP, 30DAP and 35DAP: the kernels of the 20th, 25th, 30th and 35th day after pollination of waxy corn). For each sample, the three columns are reflected light, bright-field and overlaid images.

Figure 3. (A) FTIR patterns, (B) XRD patterns, (C) double-logarithmic SAXS patterns, and (D) one-dimensional correlation function profiles for starch isolated from waxy corn at different stages of kernel growth (20DAP, 25DAP, 30DAP and 35DAP: the kernels of the 20th, 25th, 30th and 35th day after pollination of waxy corn).

Figure 4. Pasting results of starch isolated from waxy corn at different stages of kernel growth. (20DAP, 25DAP, 30DAP and 35DAP: the kernels of the 20th, 25th, 30th and 35th day after pollination of waxy corn).

Figure 5. (A) Pearson correlation coefficients of the structural and digestibility parameters of waxy corn starch; (B) Overview of the relationship between the structural changes and the digestibility of starch isolated from waxy corn at different stages of kernel growth.

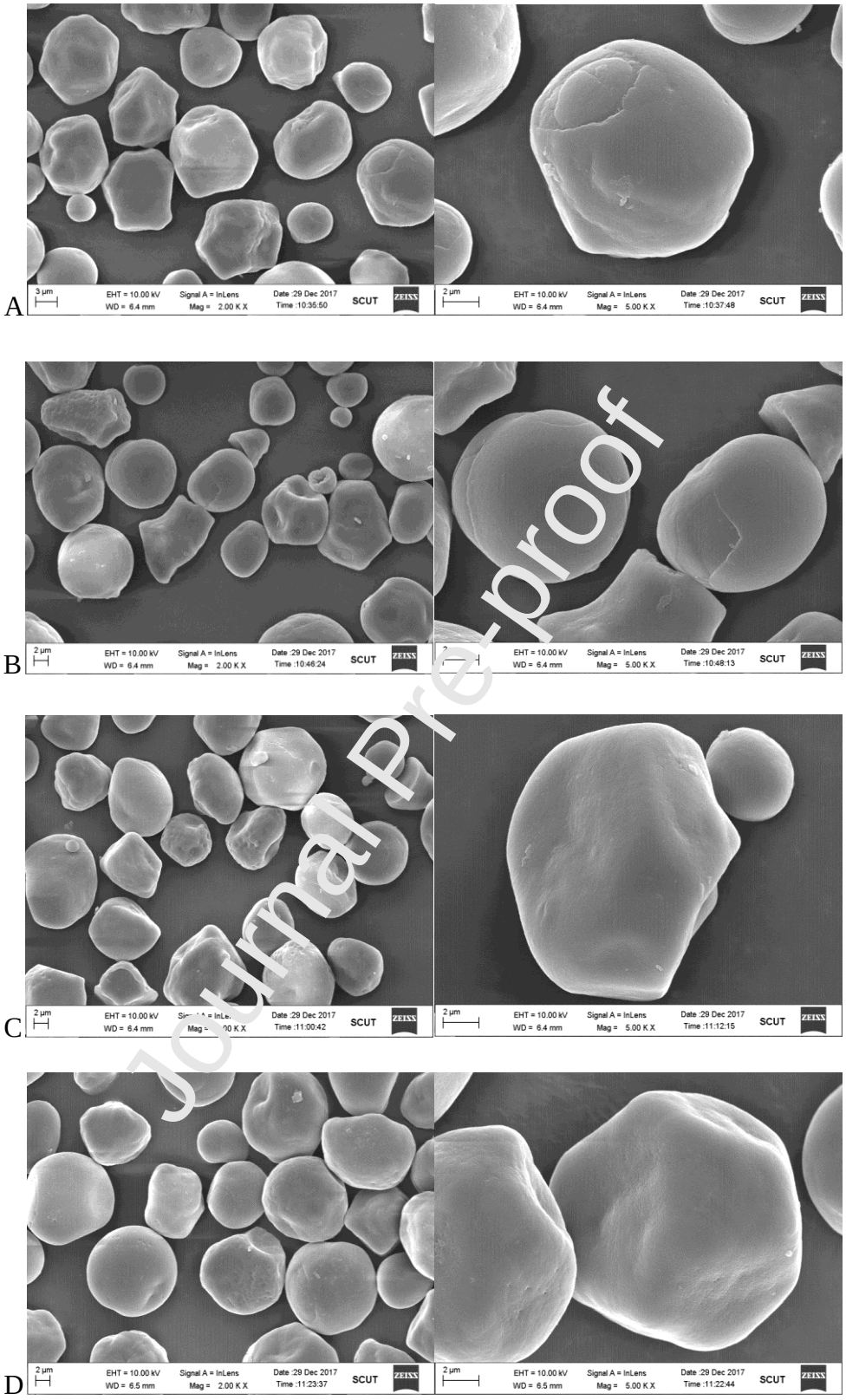

Figure 1

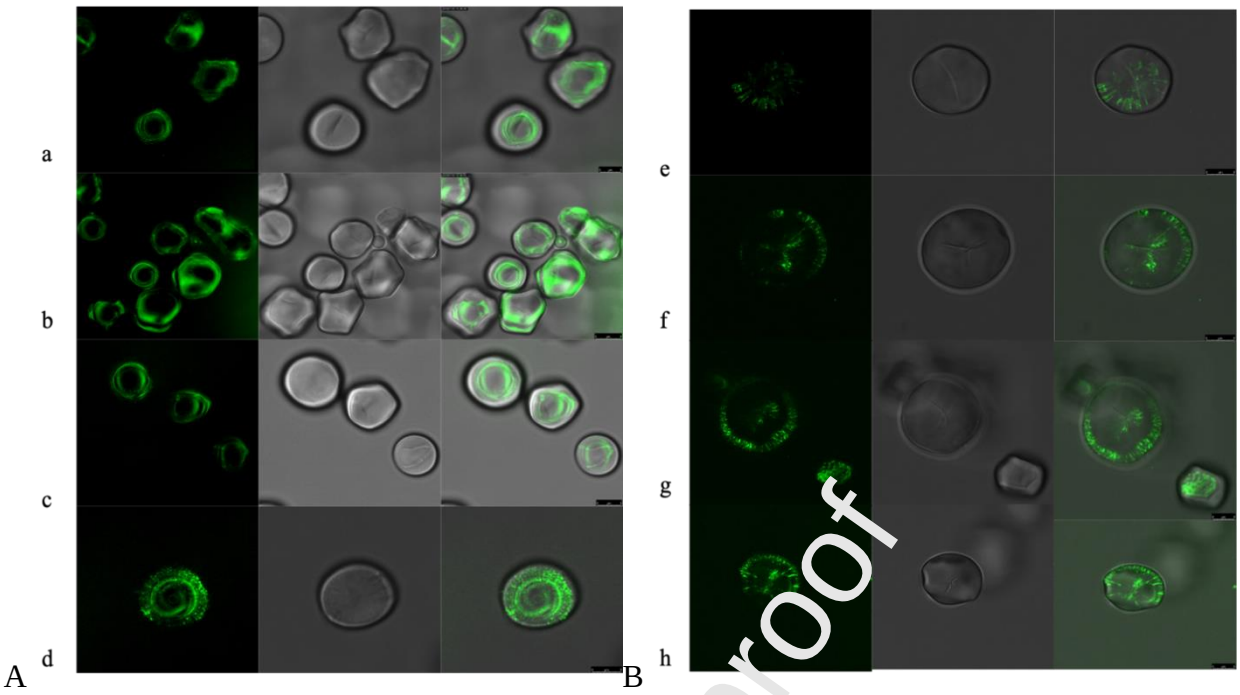

Figure 2

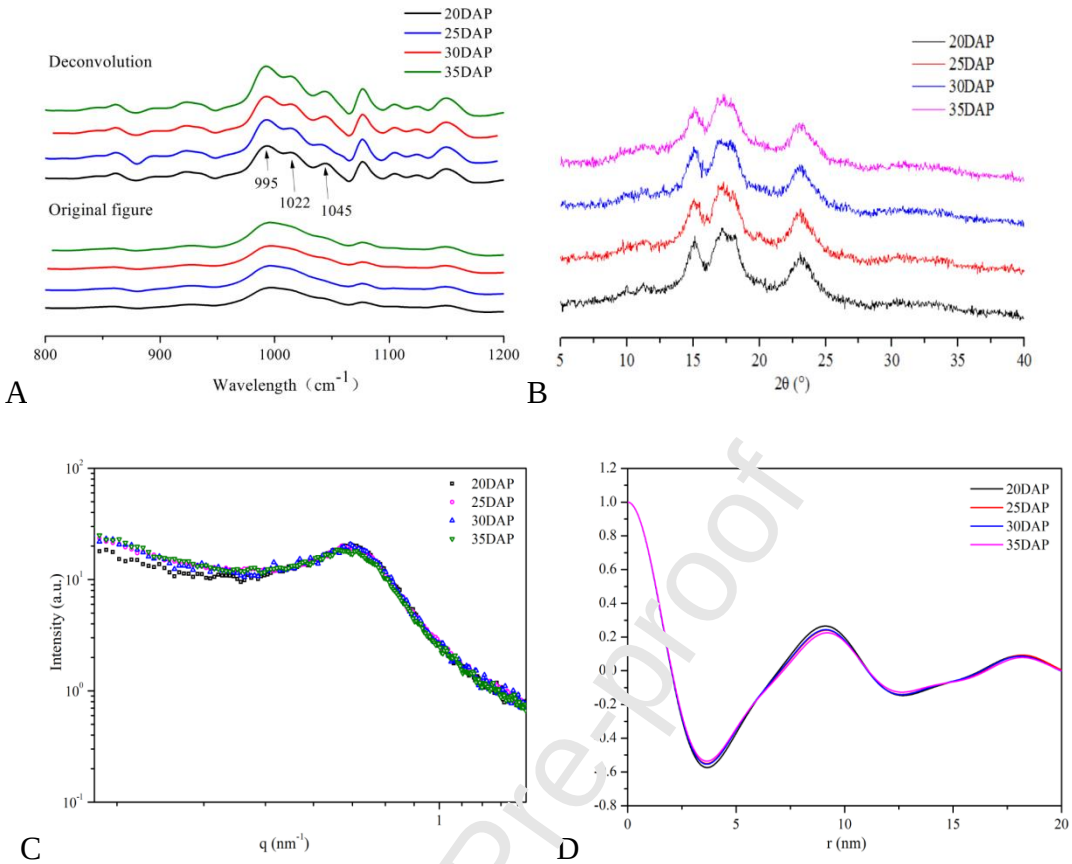

Figure 3

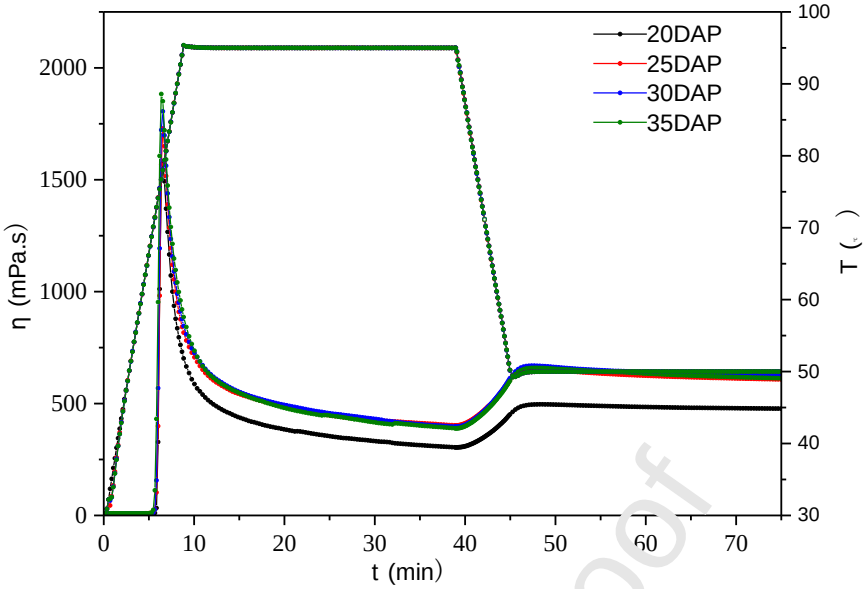

Figure 1

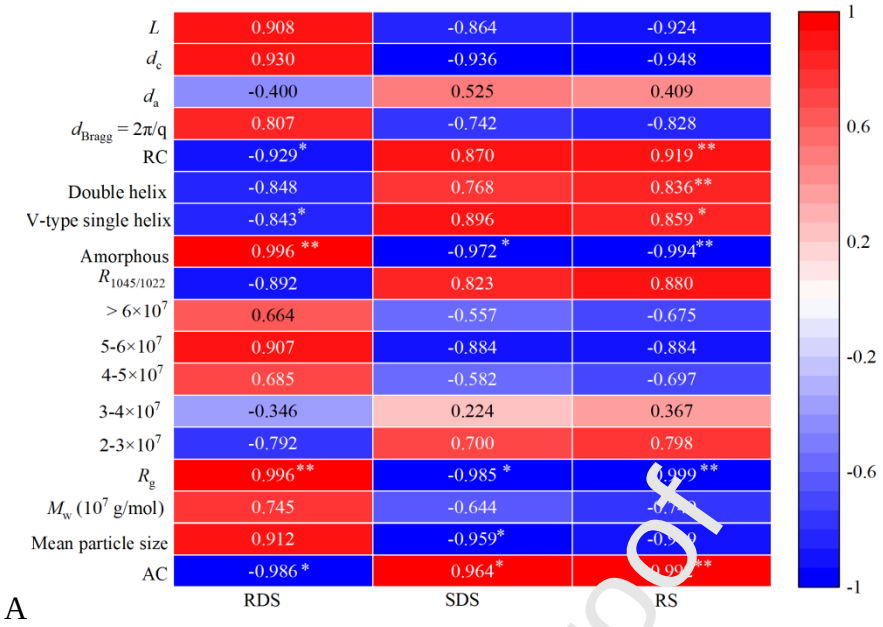

A

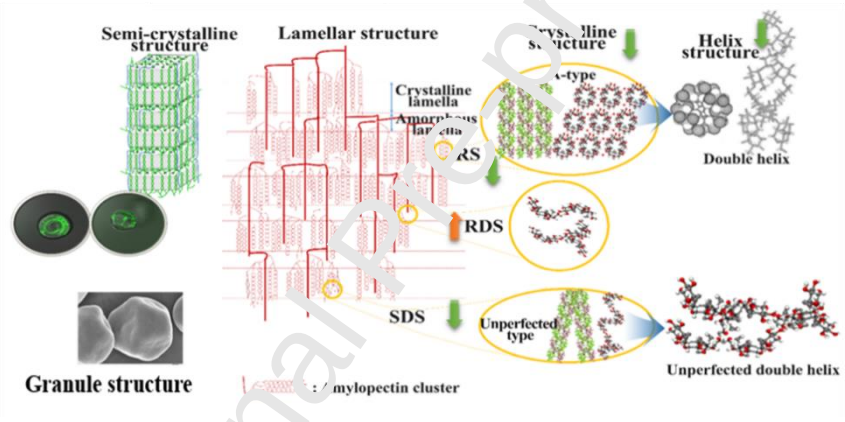

B

Figure 5

Table 1 Chemical composition of starch isolated from waxy corn at different stages of kernel growth.

Sample	Moisture (%)	Protein (%)	Lipid (%)	Ash (%)
20DAP	10.3±0.1	0.43±0.06	2.48±0.14	1.40±0.12
25DAP	10.5±0.2	0.48±0.03	2.42±0.18	1.36±0.09
30DAP	10.3±0.6	0.52±0.11	2.72±0.22	1.39±0.06
35DAP	10.6±0.2	0.56±0.03	3.02±0.17	1.34±0.14

Table 2 Amylose content, mean granule size, molecular mass, R_g, and molecular mass distribution results of starch isolated from waxy corn at different stages of kernel growth.

Sample	AC (%)	Mean granule size (μm)	M_w (10^7 g/mol)	M_n (10^7 g/mol)	R_g (nm)	Molecular mass distribution (%)				
						2–3×10^7 g/mol	3–4×10^7 g/mol	4–5×10^7 g/mol	5–6×10^7 g/mol	> 6×10^7 g/mol
20DAP	3.90±0.20[a]	10.956±0.016[c]	2.745 (1%)[c]	4.516 (1%)[a]	122.7 (1%)[c]	72.00	13.71	8.44	5.77	0
25DAP	2.70±0.10[b]	11.916±0.032[b]	2.677 (2%)[c]	2.651 (2%)[b]	141.6 (1%)[b]	57.29	15.63	11.19	5.89	0
30DAP	2.10±0.20[c]	12.203±0.028[a]	3.122 (1%)[b]	3.090 (2%)[b]	153.0 (1%)[a]	56.58	21.89	10.90	10.63	0
35DAP	1.20±0.10[d]	12.109±0.045[a]	5.336 (1%)[a]	4.895 (1%)[a]	162.9 (1%)[a]	0	0	79.55	10.57	9.88

*Means with different letters in the same column are significantly different ($p < 0.05$). AC, amylose content.

Table 3 Proportions of helices, degree of short-range order, relative crystallinity (RC), and lamellar structure parameters of starch isolated from waxy corn at different stages of kernel growth.

Sample	$R_{1045/1022}$	Amorphous starch content (%)	V-type single helix content (%)	Double helix content (%)	RC (%)	$d_{Bragg} = 2\pi/q$ (nm)	d_a (nm)	d_c (nm)	L (nm)
20DAP	0.634±0.060[a]	47.7±0.2[d]	5.9±0.1[a]	46.4±0.4[a]	35.22±0.17[b]	9.33±0.00[b]	2.86±0.02[a]	6.25±0.04[b]	9.11±0.02[b]
25DAP	0.638±0.032[a]	51.9±0.1[c]	0	47.1±0.3[a]	34.91±0.14[a]	9.45±0.00[b]	2.83±0.01[b]	6.32±0.00[b]	9.15±0.01[b]
30DAP	0.560±0.015[b]	56.3±0.1[b]	0	43.7±0.3[b]	32.54±0.18[b]	9.41±0.00[b]	2.83±0.01[b]	6.32±0.01[b]	9.15±0.01[b]
35DAP	0.499±0.027[c]	59.4±0.3[a]	0	40.6±0.1[c]	30.73±0.09[c]	9.64±0.01[a]	2.85±0.00[a]	6.35±0.00[a]	9.20±0.00[a]

*Means with different letters in the same column are significantly different ($p < 0.05$); RC, relative crystallinity.

Table 4 Pasting properties and digestibility of starch isolated from waxy corn at different stages of kernel growth.

Samples	T_p (°C)	η_{pk} (cp)	η_{sc} (cp)	η_{ec} (cp)	η_f (cp)	η_{sb} (cp)	RDS (%)	SDS (%)	RS (%)
20DAP	71.37	1574.2	304.35	451.37	477.31	147.02	40.26±0.31^{c}	44.01±0.33^{a}	16.73±0.12^{a}
25DAP	68.78	1729	402.74	605.19	607.89	202.45	44.12±0.53^{b}	42.33±0.20^{b}	13.55±0.03^{b}
30DAP	68.79	1805.6	396.81	613.23	625	216.42	47.58±0.17^{c}	41.10±0.22^{c}	11.32±0.29^{c}
35DAP	67.44	1883.1	389.72	601.08	613.02	211.36	49.3[illegible]±0.[illegible]^{c}	40.88±0.28^{c}	9.80±0.10^{d}

*T_p, pasting temperature; $\eta_{pk,}$ peak viscosity; η_{sc}, viscosity at the start of cooling (95 °C); η_{ec}, viscosity at the end of cooling; η_f, final viscosity; η_{sb} (= $\eta_{ec} - \eta_{sc}$), setback viscosity; RDS, rapidly digestible starch; SDS, slowly digestible starch; RS, resistant starch; Means with different letters in the same column are significantly different ($p < 0.05$).

CRediT author statement:

Bo Zheng: Methodology, Validation, Formal analysis, Investigation, Data Curation, Writing - Original Draft, Visualization. **Xinbo Guo:** Methodology**,** Formal analysis, Writing &Review, **Yukuo Tang**: Methodology, Investigation, Data Curation**. Ling Chen:** Conceptualization, Methodology, Resources, Supervision, Project administration, Funding acquisition. **Fengwei Xie**: Methodology, Resources, Writing - Review & Editing, Visualization.

Highlights

- Waxy corn starch chain (WCS) structure changed largely during kernel growth
- The amylose and double helix contents of WCS decreased during kernel growth
- The digestibility of WCS increased in relation to kernel development
- Kernel development increased paste viscosity but reduced paste cooling stability